Molecular Crystals and Liquid Crystals

Publication details, including instructions for authors and subscription information:
http://www.tandfonline.com/loi/gmcl20

High Resolution ADF-STEM Imaging Application for Organic Crystals

Mitsutaka Haruta [a], Kaname Yoshida [a], Hiroki Kurata [a] & Seiji Isoda [a]

[a] Institute for Chemical Research, Kyoto University, Uji, Kyoto, Japan

Version of record first published: 31 Aug 2012.

To cite this article: Mitsutaka Haruta , Kaname Yoshida , Hiroki Kurata & Seiji Isoda (2008): High Resolution ADF-STEM Imaging Application for Organic Crystals, Molecular Crystals and Liquid Crystals, 492:1, 200/[564]-209/[573]

To link to this article: http://dx.doi.org/10.1080/15421400802330663

Mol. Cryst. Liq. Cryst., Vol. 492, pp. 200/[564]–209/[573], 2008

ISSN: 1542-1406 print/1563-5287 online
DOI: 10.1080/15421400802330663

Taylor & Francis
Taylor & Francis Group

High Resolution ADF-STEM Imaging Application for Organic Crystals

Mitsutaka Haruta, Kaname Yoshida, Hiroki Kurata, and Seiji Isoda
Institute for Chemical Research, Kyoto University, Uji, Kyoto, Japan

High-resolution annular dark-field scanning transmission electron microscopy (ADF-STEM) imaging was applied for structural observations of organic crystals so as to achieve quantitative atomically resolved images. In particular, a low angle annular dark-field method (LAADF-STEM) was found to be highly advantageous for radiation sensitive organic materials, because stronger thermal diffuse scatterings can be utilized for imaging. So called quantitative Z-contrast images of organic molecules at atomic resolution were demonstrated in several organic crystals.

Keywords: ADF-STEM; electron microscopy; high resolution; organic materials

INTRODUCTION

In the annular dark-field scanning transmission electron microscopy (ADF-STEM), a finely focused electron probe is scanned on a sample surface. When electrons scattered at higher angular region than about 50 mrad are detected by high-angle annular detector, a high resolution dark-field image (HAADF-STEM) is formed. In this case, the detected electrons are primarily attributable to the thermal diffuse scattering (TDS), suggesting that the image is formed incoherently and its contrast depends on atomic numbers of elements in sample (Z-contrast) [1]. Intensity of HAADF-STEM is known to be proportional to $Z^{1.7–2.0}$ in many cases. In contrast to a transmission electron microscopy (TEM) experiment, HAADF-STEM imaging is much less sensitive to the experimental conditions; therefore, the image can be intuitively interpreted as seen in the images. By employing these characteristics, high-resolution

Address correspondence to Mitsutaka Haruta, Institute for Chemical Research, Kyoto University, Uji, Kyoto 611-0011, Japan. E-mail: haruta@eels.kuicr.kyoto-u.ac.jp

HAADF-STEM imaging experiments have been performed invariably on inorganic crystals, including defect [2,3], interfaces [4–6], and surfaces [7], in which atomic positions of relatively heavy elements have been successfully visualized. The recent development of a spherical aberration corrector for an illuminating lens system enables observation of even oxygen atoms in inorganic crystals using the HAADF-STEM method [8]. However, the ADF-STEM such as HAADF-STEM has not been utilized for atomic imaging of organic crystals, presumably due to the weakness of organic crystals against strong electron irradiation, especially under a focused electron beam in the ADF-STEM. This may further be attributed to the fact that organic molecular crystals are composed of light elements such as carbon and nitrogen.

In our recent work, ADF-STEM measurement have demonstrated for the first time that the method can be applicable for acquiring Z-contrast images of organic molecular crystal structures at atomic resolution in a case of hexadecachloro-Cu-phthalocyanine (Cl_{16}-CuPc) [9]. In the report, it has been emphasized that another ADF-STEM of low-angle annular dark field STEM (LAADF-STEM) is highly advantageous in taking images when radiation sensitive organic materials are observed, as mention later. The LAADF-STEM images are formed by electrons scattered at lower angular region from 30 mrad to 60 mrad.

Since Uyeda *et al.* have reported the first successful observation of the structural image of organic molecular crystals at atomic resolution by TEM [10], many high-resolution TEM studies have been performed for organic materials [11]. A main problem in TEM, however, is its low property in quantitative image contrast, owing to coherent imaging. Therefore, it is an important subject to apply the ADF-STEM, especially LAADF-STEM, for quantitative examination on structures of organic crystals.

EXPERIMENTAL

In the present study, LAADF-STEM observation was applied to five kinds of organic crystals; silver phthalocyanine (AgPc), chlorotetraphenylporphinate-Fe (ClTPPFe), poly-germanium-oxy-phthalocyanine ($(GeOPc)_n$), bis(1,4-diphenylglyoximato)platinum ($Pt(dpg)_2$) and polyhalogenated CuPc (substituted as $Br_{13}Cl_3$-CuPc on an average). AgPc, ClTPPFe, $(GeOPc)_n$, and $Pt(dpg)_2$ suffer nearly the same degree of radiation damage; their total end-point dose (TEPD), based on measurements of the decrease in diffraction intensity, are about 0.1–1.0 C/cm^2 but that of $Br_{13}Cl_3$-CuPc is much larger up to 30 C/cm^2. . These molecules were prepared so as to examine effects of radiation damage in LAADF-STEM imaging.

TABLE 1 Conditions of the Vacuum Deposition for Organic Molecular Crystals

Material	Substrate crystal	Temperature of substrate (°C)
$Br_{13}Cl_3$-CuPc	KCl	320
Pt(dpg)2	KI	70
FeCllTPP	KBr	130
AgPc	KBr	205
GeOPc	KCl	200

STEM samples were prepared as thin films on (001)-cleaved surfaces of alkali halide single-crystals by vacuum vapor deposition [12–15]. Prior to the deposition, the substrates were heated at 400°C for one hour in order to remove adsorbed water and other contaminants. The temperature of substrate was maintained at each optimal temperature during the deposition, and the thickness of deposited layers was controlled to be several tens of nanometer by monitoring the deposition rate using a quartz microbalance. Table 1 summarizes each optimal condition of deposition. The thickness of films was measured using an atomic force microscope (AFM). The cross-sectional profiles of the AFM image indicate that all the films were composed of flat crystallites with nearly the same thickness (40 to 70 nm). The each molecular crystal formed on the substrate was covered with a thin amorphous carbon film for high-resolution LAADF-STEM imaging. After the alkali halide substrate was subsequently removed from the surface on distilled water, the sample was fixed on a microgrid.

ADF-STEM observation was performed at room temperature using a 200 kV TEM/STEM (JEM-2200FS, JEOL) equipped with a Schottky emission gun. The annular detection angle was set at 24–64 mrad by choosing a camera length of 12 cm, corresponding to LAADF-STEM imaging rather than HAADF-STEM (typical detection angular range of 50–170 mrad).

RESULTS AND DISCUSSION

The elastic scattering intensity I^{BS} and TDS I^{TDS} can be expressed respectively as $I^{BS} = |f_x(s)|^2 \exp[-2M_x(s)]$ and $I^{TDS} = |f_x(s)|^2\{1-\exp[-2M_x(s)]\}$, where $s = sin(\theta)/\lambda$, f_x(s) and M_x(s) are the atomic structure factor for electron and the temperature factor of each element x, respectively. When assuming the Einstein type thermal motion, $M_x(s) = Bs^2$. Figure 1 shows the intensity profiles of the elastic scattering and TDS for an isolated C, N, Cl, Cu, and Br atoms under the

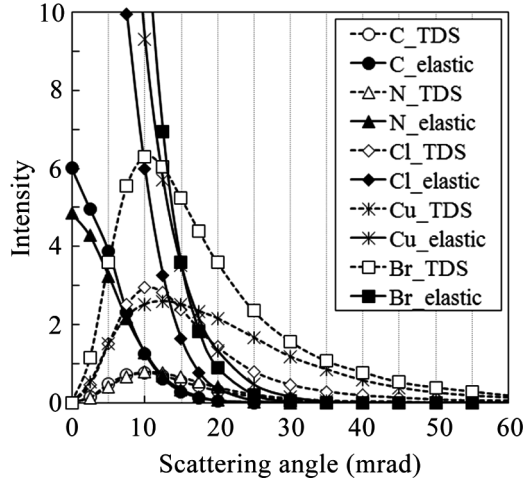

FIGURE 1 Intensity profiles of elastic and thermal diffuse scatterings (TDS) from isolated C, N, Cl, Cu, and Br atoms under Einstein model. The crossover point between elastic and TDS profiles is found at scattering angle of about under 20 mrad for each atom. The LAADF-STEM detecting electrons scattered above 30 mrad guarantees to collect almost only TDS signals in case of organic materials.

assumption of Einstein type thermal motion. The Debye-Waller factor for each element was assumed the value used in the mulislice image simulation for halogenated-CuPc [9]. As shown, heavier atoms exhibit higher TDS as well as elastic components. Since each Debye-Waller factor in organic materials is large compared to that in inorganic materials, the crossover point between elastic and TDS profiles is found at scattering angle of about under 20 mrad for each atom. Owing to the large Debye-Waller factor, therefore, the LAADF-STEM detecting electrons scattered above 30 mrad guarantees to collect almost only TDS signals in case of organic materials, leading to the incoherent high resolution Z-contrast imaging. Indeed, it has been demonstrated that the LAADF-STEM imaging is a quite good method for observation of organic materials like fullerene (C_{60}) molecules [16]. In our previous study [9], an image simulation has been carried out for Cl_{16}-CuPc crystal so as to evaluate the elastic contribution, indicating that the elastic contribution is only about 1/100 against the TDS one when Debye-Waller factor and the lattice constants are large enough. On the other hand, the image intensities of organic materials are very weak compared to inorganic material in case of conventional HAADF-STEM condition (detecting above 50 mrad), so that the HAADF-SETM is not

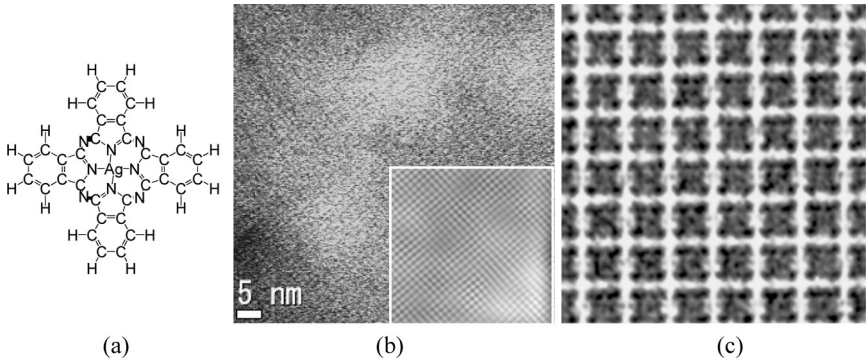

FIGURE 2 (a) Molecular structures of AgPc. (b) Observed LAADF-STEM image of AgPc along the c-axis. The inset image is a noise-filtered image by Fourier filtering. (c) TEM image of AgPc, in which the molecular shape seems clearer but the image contrast is no more quantitative.

easily applicable for radiation sensitive materials. Consequently, the LAADF-STEM should be a powerful technique to analyze organic structures with large Debye-Waller factor and large unit cells.

The LAADF-STEM was applied to observe the structures of AgPc, ClTPPFe, $(GeOPc)_n$ and $Pt(dpg)_2$. These molecules have the central coordinated atoms of Ag ($Z = 47$), Cl + Fe ($Z = 26 + 17$), Ge + O ($Z = 32 + 8$) and Pt ($Z = 78$) along the atomic columns. Figure 2(b) shows an observed LAADF-STEM image of AgPc at a magnification of 1.5 M projected along the Ag column in the c-axis. The inset is a noise-filtered image by Fourier filtering, where the bright contrasts seem to build a unit cell network and then the bright contrasts are referable to the Ag columns at the center of each molecule, even though no other contrasts are observed due to the radiation damage. On the other hand, a conventional TEM image demonstrates relatively clear shape of the molecule as shown in Figure 2(c). However, the contrast of Ag is almost similar or even weaker than other parts of molecules, meaning no quantitative contrast of atoms. Therefore there is no direct way to identify the species of the central atom by TEM.

The $(GeOPc)_n$ crystal has a tetragonal crystal with lattice dimensions of $a = b = 1.372\,\text{nm}$ and c (chain axis) $= 0.66\,\text{nm}$ [12,13]. Figure 3(b) shows observed LAADF-STEM image of $(GeOPc)_n$ at a magnification of 2.5 M projected along the c-axis and the inset is a noise-filtered image. Here again the bright contrasts correspond to the unit cell alignment, so that the bright contrasts should be originated from the Ge + O atomic columns at the center of each molecule. Since this material as well as AgPc, ClTPPFe (not shown) and $Pt(dpg)_2$

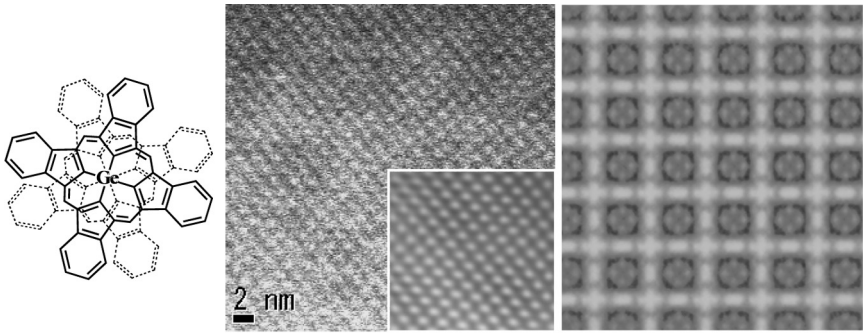

FIGURE 3 (a) Molecular structures of $(GeOPc)_n$ projected along the chain axis. Staggering angle is 37°. (b) Observed LAADF-STEM image of $(GeOPc)_n$. The inset image is a noise-filtered images by Fourier filtering. (c) The corresponding TEM image is again not quantitative even though the molecular shape seems clear.

(not shown) is sensitive to electron irradiation compared to $Br_{13}Cl_3$-CuPc described later, more high-magnification observations was very difficult, resulting into a low resolution. Corresponding TEM image of $(GeOPc)_n$ is shown in Figure 3(c), in which the intensity of the Ge-O chain at molecular center is very weak and peripheral parts of the molecule appear with rather stronger contrast. This demonstrates also the disadvantage of TEM imaging.

In the TEM imaging, an operator adopts commonly a radiation minimization technique like a minimum dose system so as to avoid unnecessary electron irradiation on a specific area in specimen and to irradiate on the objective area only during exposure [17,18]. However, in the present STEM case, we have no such specialized technique to minimize radiation damage, but the electrons were continuously falling on the specimens during adjustments of crystal orientation and electron optics in addition to exposure. This is another reason of low resolution in STEM images, and one needs to develop a radiation minimization system to realize higher resolution.

In AgPc, $(GeOPc)_n$, ClTPPFe and $Pt(dpg)_2$, heavy atomic chains are imaged with stronger contrast, but the sizes of the contrasts are relatively larger from those expected from multislice simulations. This indicates a possibility that the images could be affected by electron radiation damage, molecular channeling and molecular vibration.

The crystal structure of a polyhalogenated-CuPc, $Br_{13}Cl_3$-CuPc with stronger resistance to electron irradiation than the above

materials, was observed by LAADF-STEM. The image is compared with the previous result of Cl_{16}-CuPc [9]. The each molecules are packed in a base-centered monoclinic structure isomorphic to Cl_{16}-CuPc and Br_8Cl_8-CuPc, with unit-cell dimensions of $a = 1.962$ nm, $b = 2.604$ nm, $c = 0.376$ nm, and $\beta = 116.5^\circ$ [19]. The a–b plane of the monoclinic structure (i.e., molecular planes) is parallel to the substrate surface as expected for vacuum deposition.

As $Br_{13}Cl_3$-CuPc is still radiation sensitive, the crystal orientation was required to be adjusted as quickly as possible. The radiation damage to the halogenated-CuPc was estimated to be $30\,C/cm^2$ as a total end-point dose. Since the TDS intensity is expected to be low at higher angles in these specimens as shown in Figure 1, high-resolution HAADF-STEM observations would be very difficult (but it is yet possible at some level to observe high-resolution images by HAADF-STEM in this material). Therefore, observations under the conditions of LAADF-STEM were attempted in order to utilize the stronger TDS intensity as mentioned already. To realize high-resolution LAADF-STEM images, the 12 cm camera length (detection angle: 24–64 mrad) corresponding to LAADF imaging was applied. This detection angular range was found to provide incoherent Z-contrast images as in the commonly employed HAADF-STEM cases, which can be verified from the multislice image simulation [9]. As a result, this detection angle ensures that incoherent imaging becomes dominant even in LAADF condition; LAADF-STEM observation proves indeed quantitative information from organic molecular crystal.

A typical experimental LAADF-STEM image of $Br_{13}Cl_3$-CuPc molecular crystal is shown in Figure 4(b) together with a noise-filtered image in the inset of the figure. The experimental image is strongly deteriorated by noises, probably due to the weakness of the detected signals at a magnification of 3 M, in addition to electron radiation damage and a noise from the supporting carbon film. In the noise-filtered image, the central Cu columns and the peripheral halogen atom columns in the molecules can be observed clearly with almost the same contrast, which corresponds well the ratio between the atomic numbers in Cu ($Z = 29$) and Br + Cl ($Z_{ave} = 31.6$ 31.6 by assuming random substitution). However, light elements such as the C and N columns are invisible in these images, presumably due to the narrow dynamic range of the detector employed in the limited spatial resolution of the present experiment. Figure 4(c) shows a LAADF-STEM image of Cl_{16}-CuPc, where the halogenated positions appear weaker contrast than that of the central Cu, being controlled by Z-contrast. Contrarily to this, a TEM image of

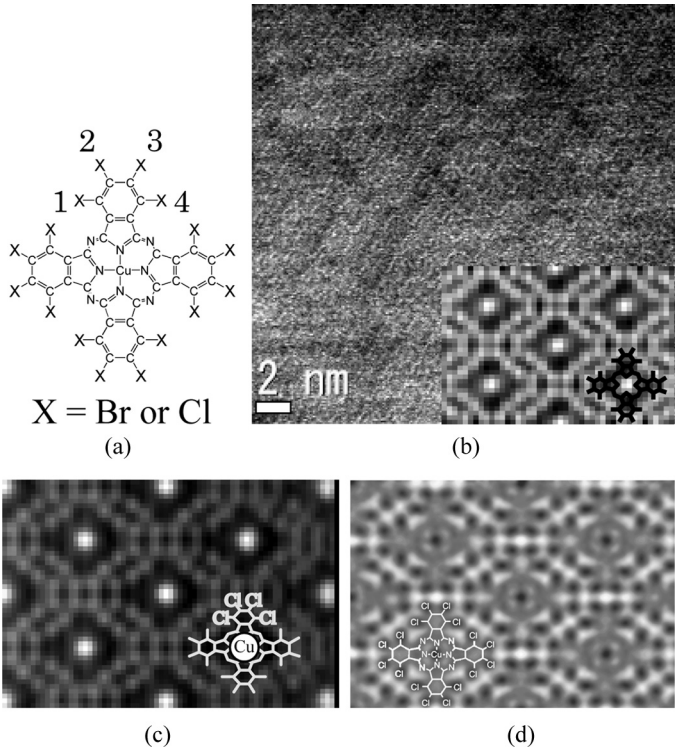

FIGURE 4 (a) Molecular structure of polyhalogenated CuPc with Br and Cl at positions 1–4 (X = Br, Cl); $Br_{13}Cl_3$-CuPc. (b) Observed LAADF-STEM image of $Br_{13}Cl_3$-CuPc. The inset image is a noise-filtered image by Fourier filtering where the contrasts at Cu and halogen sites are nearly the same as expected. (c) LAADF-STEM image of Cl_{16}-CuPc and (d) the corresponding TEM image in which the contrast at Cl is almost the same to that of Cu. However, LAADF-STEM image (c) shows stronger contrast at Cu position than Cl depending quantitatively to their Z numbers.

Cl_{16}-CuPc exhibits similar contrasts on the Cu and Cl positions as shown in Figure 4(d), indicating obviously disadvantage on quantitative image analysis in TEM. In comparison with the TEM images, the LAADF-STEM is powerful tool to identify quantitatively atomic species in specimens at atomic scale, especially for organic materials, and moreover it should be emphasized that the ADF-STEM, including HAADF- and LAADF-STEM, is expected to realize higher resolution than TEM due to incoherent imaging theoretically.

CONCLUDING REMARKS

High resolution Z-contrast images of organic molecular crystals at atomic resolution were obtained by LAADF-STEM. In molecular crystals with comparatively large Debye-Waller factor and large lattice constants, LAADF-STEM observation with a lower detection angle of 24–64 mrad was found to be advantageous for acquiring incoherent Z-contrast images similar to the case of conventional HAADF-STEM, as verified by multislice image simulation.

LAADF-STEM observation was applied to the many organic molecular crystals. It was only visible the heavier atomic columns at the center of each molecule in many cases. Although LAADF-STEM observation is useful for study on organic molecular crystals, unnecessary electron irradiation is a serious problem inherent in STEM observation of radiation-sensitive materials. In order to achieve higher resolution for organic crystals by ADF-STEM, unnecessary irradiation should be minimized, by developing a minimum dose system with shutter function and/or with a finer electron probe. Such a system would promise lower-dose observation for organic crystals and allow imaging at higher spatial resolution.

REFERENCES

[1] Nellist, P. D. & Pennycook, S. J. (2000). *Advances in Imaging and Electron Physics*, *113*, 147.
[2] McGibbon, A. J., Pennycook, S. J., & Angelo, J. E. (1995). *Science*, *269*, 519.
[3] Batson, P. E. (2000). *Phys. Rev. B.*, *61*, 16633.
[4] McGibbon, M. M., Browning, N. D., Chisholm, M. F., McGibbon, A. J., Pennycook, S. J., Ravikumar, V., & Dravid, V. P. (1994). *Science*, *266*, 102.
[5] Browning, N. D. & Pennycook, S. J. (1996). *J. Phys. D: Appl. Phys.*, *29*, 1779.
[6] Xin, Y., Pennycook, S. J., Browning, N. D., Nellist, P. D., Sivananthan, S., Omnès, F., Beaumont, B., Faurie, J. P., & Gibart, P. (1998). *Appl. Phys. Lett.*, *72*, 2680.
[7] Wang, C. M., Zhang, Y., Shutthanandan, V., Baer, D. R., Weber, W. J., Thomas, L. E., Thevuthasan, S., & Duscher, G. (2005). *Phys. Rev. B.*, *72*, 245421.
[8] Pennycook, S. J., Varela, M., Hetherington, C. J. D., & Kirkland, A. I. (2006). *MRS Bulletin.*, *31*, 36.
[9] Haruta, M., Yoshida, K., Kurata, H., & Isoda, S. (2008). *Ultramicroscopy*, *108*, 545.
[10] Uyeda, N., Kobayashi, T., Ishizuka, K., & Fujiyoshi, Y. (1979). *Chemica Scripta*, *14*, 47.
[11] Kobayashi, T. (1991). In: *Crystal, Growth, Properties and Application*, Karl, N. (Ed.), Springer Verlag: Berlin, Heidelberg, Vol. 13, 2.
[12] Isoda, S., Kubo, I., Hashimoto, A., Asaka, N., Kurata, H., & Kobayashi, T. (1991). *J. Cryst. Growth*, *115*, 388.
[13] Kobayashi, T. & Uyeda, N. (1987). *J. Cryst. Growth*, *84*, 589.
[14] Isoda, S., Tsujimoto, M., Yoshida, K., Kobayashi, Y., & Kamata, T. (1998). *Mol. Cryst. Liq. Cryst.*, *316*, 15.

[15] Kamata, T., Fukaya, T., Matsuda, H., Mizukami, F., & Tachiya, M. (1995). *J. Phys. Chem.*, *99*, 13239.
[16] Haruta, M., Yoshida, K., Kurata, H., & Isoda, S. (2006). *Proceedings of IMC 16th*, 1791.
[17] Fujiyoshi, Y., Kobayasti, T., Uyeda, N., Ishida, Y., & Harada, Y. (1980). *Ultramicroscopy*, *5*, 459.
[18] Wrigley, G., Brown, E., & Chillingworth, P. K. (1983). *J. Microscopy*, *130*, 225.
[19] Uyeda, N., Kobayashi, T., Suito, E., Harada, Y., & Watanabe, M. (1972). *J. Appl. Phys.*, *43*, 5181.